

Hierarchical Bayesian integrated modeling of age- and sex-structured wildlife population dynamics

Sabyasachi Mukhopadhyay^{1,2}, Hans-Peter Piepho¹, Sourabh
Bhattacharya³, Holly T. Dublin⁴, Joseph O. Ogutu¹

¹*University of Hohenheim, Institute of Crop Science, Biostatistics Unit (340C),
Fruwirthstrasse 23,
70599 Stuttgart Germany*

²*Indian Institute of Management, Udaipur, India*

³*ISRU, Indian Statistical Institute,
203, B.T. Road, Kolkata-108, India*

⁴*IUCN ESARO, Wasaa Conservation Centre,
P.O. Box 68200, Nairobi, Kenya, 00200*

*Email for correspondence: mukhopad@uni-hohenheim.de,
sabyamstat@gmail.com, sabyasachi.mukhopadhyay@iimu.ac.in*

December 21, 2021

Abstract

Biodiversity of large wild mammals is declining at alarming rates world-wide. It is therefore imperative to develop effective population conservation and recovery strategies. Population dynamics models can provide insights into processes driving declines of particular populations of a species and their relative importance. Accordingly, we develop an integrated Bayesian state-space population dynamics model for wildlife populations and illustrate it using a topi population inhabiting the Masai Mara Ecosystem in Kenya. The model is general and integrates ground demographic survey with aerial survey monitoring data. It incorporates population age- and sex-structure and life-history traits and strategies and relates birth rates, age-specific survival rates and sex ratios with meteorological covariates, prior

population density, environmental seasonality and predation risk. It runs on a monthly time step, enabling accurate characterization of reproductive seasonality, phenology, synchrony and prolificacy of births, juvenile and adult recruitments. Model performance is evaluated using balanced bootstrap sampling and by comparing model predictions with empirical aerial population size estimates. The hierarchical Bayesian model is implemented using MCMC methods for parameter estimation, prediction and inference and reproduces several well-known features of the Mara topi population, including striking and persistent population decline, seasonality of births, juvenile and adult recruitments. It is general and can be readily adapted for other wildlife species and extended to incorporate several additional useful features.

Keywords: Bayesian modelling, animal population dynamics, birth and juvenile recruitment rates, integrated state-space model, Markov Chain Monte Carlo, survival rates and sex ratio.

1 Introduction

Biodiversity is declining worldwide at such an alarming rate that biologists have christened the contemporary biodiversity loss as the sixth mass extinction (Ceballos et al., 2017; McCallum, 2015). Large mammal populations are particularly at risk in many ecosystems. Across continental Africa, many populations of large mammal species are undergoing disturbing declines (Chase et al., 2016; Craigie et al., 2010). In Kenya, for example, large herbivore populations declined by 70% on average between 1977 and 2016 (Ogutu et al., 2011, 2016). It is therefore imperative to advance our understanding of large herbivore population dynamics as a basis for developing species conservation and management and population recovery strategies. A reliable population dynamics model can help quantify and evaluate the relative importance of multiple processes driving declines of particular populations of a species.

For populations inhabiting seasonally variable environments and reproducing seasonally, such models can help quantify shifts in seasonality, phenology, synchrony and prolificacy of births, juvenile recruitment and sex ratio in response to climate and other changes. The models can also be used to estimate population trajectories and assess likely population responses to conservation and management interventions, projected future scenarios of climate change, human population

growth, socio-economic development, land use and other changes (Zhao et al., 2019a; Zhao et al., 2019b).

Animal population dynamics models often use independent data collected using various methods, such as ground demographic surveys and aerial surveys. Population dynamics models are also increasingly using information from multiple sources to make inferences on various features of populations. Notably, integrated population models are becoming widely used to combine different types of data from disparate sources to make joint inferences on animal population dynamics (Besbeas et al., 2005; Maunder et al., 2015; Mosnier et al., 2015; Rhodes et al., 2011; Trenkel et al., 2000). However, thus far, integrated state-space population dynamics models for wildlife populations that incorporate realistic life-history traits and strategies and fine temporal frames have not been developed. Yet, such models are crucial for understanding and quantifying how life-history traits and strategies shape population responses to trophic interactions, natural environmental and anthropogenic stressors.

Here, we develop an integrated population dynamics model for large wild herbivores that integrates aerial survey data with fine-resolution ground demographic survey data. The model can be used to predict large herbivore population dynamics and evaluate the relative importance of various factors driving population dynamics. It accounts for influences on large herbivore population dynamics of variation in climatic components, notably rainfall, temperature and their interactions; predation, density-dependence, population age and sex (adult sex ratio) structure, gestation length, weaning period, adult female pregnancy status, adult females available to conceive, females reaching the age of first-time conception, birth, juvenile and adult recruitment, age- and sex-specific survival rates and environmental seasonality. The model runs on a discrete monthly time step to reliably track temporal variation in female pregnancy status, birth, juvenile and adult recruitment, age and sex-specific survival rates, adult sex ratio, population size and inter-annual variation in reproductive seasonality, phenology, synchrony and prolificity of births. The model is illustrated using the topi (*Damaliscus lunatus korrigum*) population inhabiting the Masai Mara Ecosystem of south-western Kenya but is general and applicable to populations of other large herbivore species.

Our integrated state-space modelling approach has several attractive and desirable properties. (1) It integrates various data types from multiple sources, notably aerial surveys and demographic ground counts. (2) It incorporates realistic population life-history traits and strategies, survival rates, sex ratios and trophic interactions, namely predation and competition. (3) It accommodates and permits straightforward representation of possibly complex non-linear relationships

between birth and adult recruitments, age-specific survival rates, adult sex ratio and multiple covariates. (4) It predicts the ecosystem-wide population size and distributes this among the ecosystem's subregions, including those covered by the aerial surveys only. (5) The model uses a monthly time step, allowing accurate characterization of reproductive seasonality, phenology, synchrony and prolificity of birth and juvenile recruitment. (6) The model allows efficient computation of posterior distributions of many parameters and uses a flexible Transformation MCMC (TMCMC) technique to enhance computational efficiency and accelerate convergence of iterations. (7) The model is validated using balanced bootstrap sampling to generate multiple population trajectories and establish robustness. (8) It uses the Importance Resampling MCMC (IRMCMC) technique for the first time to accelerate MCMC iterations for multiple data sets each of which involves high computational costs. (9) Lastly, the model is robust and reliably reproduces well known features of animal population dynamics and can be easily adapted for other species.

The rest of the paper is organized as follows. We describe the data in Section 2. The Bayesian state-space model is described in Section 3 along with an evaluation of its performance using balanced bootstrap samples. In Section 4, we formulate the birth and adult recruitments, age-specific survival and adult sex ratio models, prior distributions and other model components. In Section 5, we discuss the convergence of the MCMC chain and model validation. In Section 6, we present results of applying the state-space model to the Mara-Serengeti topi population. Finally, in Section 7 we discuss the results and extensions of the model.

2 The data

We provide brief overviews of the data and the study population in Sections 2.1 to 2.4 and supply additional details on the vehicle ground sample counts, aerial sample surveys, the Mara-Serengeti topi population, rainfall and temperature in Web Appendices B-E. The full data dictionary providing definitions of all the variables and transformations used in the model is provided in Web Appendix A.

2.1 Ground vehicle age and sex composition sample surveys

Vehicle ground age and sex composition sample surveys of seven ungulate species, including topi, were carried out monthly in the Maasai Mara National Reserve and its adjoining pastoral lands for 174 months from July 1989 to December 2003.

Approximate ages of topi in each size class are newborn (Age < 1 month), quarter size class (1 month \leq Age < 6 months), half-yearling class (6 months \leq Age < 19 months) and adults (19 months \leq Age). Adult topi were not aged but were sexed using the presence, size and shape of horns, dimorphic morphology of the external genitalia and other secondary sexual characters. During the entire monitoring period 91,582 topi were aged and 78,738 were sexed (Ogutu et al., 2008). The age- and sex-structured topi ground counts are provided in Web Appendix A and described in Web Table 1.

2.2 Aerial sample surveys

These data are independent of the vehicle ground sample age- and sex-structured counts. The Directorate of Resource Surveys and Remote Sensing of Kenya (DRSRS) monitored wildlife population size and distribution in the Maasai Mara Ecosystem (6665.6 km²) using systematic reconnaissance flights from 1977. A total of 75 surveys were carried out in the ecosystem from 1977 to 2018 using 662 flights. The total topi population size estimated from the aerial survey data are provided in Web Appendix A and described in Web Table 2.

2.3 The Mara-Serengeti topi population

Topi is a resident grazer in the Mara–Serengeti ecosystem. There, births are seasonal, start in July and peak at the onset of the early rains in October–November, whereas conceptions peak at the start of the long rains in February–March. Births occur in all months but are rare from January to July (Sinclair et al., 2000; Ogutu et al., 2010; 2014, 2015). The gestation period of 8 months is followed by a lactation period of 3 months. Consequently, topi young are weaned after 3–4 months and nursing ceases before conceptions. Topi thus take about 11 months from one conception cycle to the next and give birth to one young per year. The young go through a hiding stage before following their mothers (Estes, 1991; Skinner and Chimimba, 2005). Females attain sexual maturity after about 18 months. Topi pregnancy rate in Mara-Serengeti is 100% for adult but 86% for 2-year-old females (Duncan, 1975).

2.4 Rainfall and temperature

In African savannas vegetation production, quantity and quality are controlled by rainfall (Deshmukh, 1984; Boutton et al., 1988a). Rainfall seasonality gener-

ates and sustains seasonality in food availability and quality for large herbivores (Boutton et al., 1988b). Accordingly, rainfall indexes food availability and quality for savanna herbivores. Seasonal temperature fluctuations additionally affect food quality for herbivores by governing the retention period of green plant leaf through the dry season. Monthly rainfall was averaged over a network of 15 monitoring gauges spread over the Mara to account for spatial variation (Mukhopadhyay et al., 2019). The monthly averages of blended satellite-station maximum and minimum temperatures data for each $5 \text{ km} \times 5 \text{ km}$ grid cell in the Mara Ecosystem were also extracted from the Chirps data (Funk et al., 2015) and used as covariates. The rainfall and temperature components, the months covered by each component, moving averages, lags and lagged moving averages computed for each component and used as predictors of birth and recruitments, survival probabilities and adult sex ratio are described in Web Table 3.

3 The integrated population dynamics state-space model

We construct a general age- and sex-structured population dynamics model for large wild herbivores. The model uses the number of animals observed in the ground and aerial surveys (Sections 2.1 and 2.2) that are only samples from the unobserved true population about which we wish to make inferences. Thus, the population dynamics model entails two parallel but connected processes. The first is the unobserved true population that evolves over time (called state process) and the second is the variation in the observed counts over time (called observation process). A common approach to modelling both processes simultaneously is to use state-space models (Thomas et al., 2005; Buckland et al., 2007; Newman et al., 2009; Newman et al., 2014; Maunder et al., 2015).

We develop an integrated population dynamics state-space model which couples a hypothetical (or latent) mechanistic model of large herbivore population dynamics (state process model), with a statistical observation model of aerial survey and ground demographic data (observation process model). In the state-space model, the state process model predicts the true but unknown future state of the large herbivore population given its current state. The observation model weights the predictions by the likelihood of the data and thus links the process model to the observations. Consequently, the model integrates the aerial survey monitoring data with the contemporaneous but independent ground demographic survey data.

The state-space model involves quantifying birth recruitment and survival rates of various age and sex classes of the population and sex ratio as functions of climatic factors (e.g., rainfall and temperature), intraspecific competition, population density, predation and seasonality. Our state-space model shares similarities with the general approaches proposed by Buckland et al. (2004) and Newman et al. (2006; 2014) but also has some notable differences. In particular, we make different distributional assumptions for the initial states and the other components of the state and observation processes. Most crucially, our approach differs from theirs with respect to several structural assumptions and our proposal to model transition probabilities of the state process using log-linear models in which covariates such as rainfall, temperature and population density are used as predictors of birth recruitment and survival probabilities and adult sex ratio, similar to the Bayesian approach of Brooks et al. (2004). Also, unlike Newman et al. (2006), we illustrate our model using a non-migratory species but the model can be easily adapted for migratory species. Lastly, our model incorporates several key life-history traits and strategies crucial to understanding large herbivore population biology and dynamics and uses rare long-term fine-resolution ground demographic and aerial survey monitoring data.

In Sections 3.1 to 4.4, we describe the state process and observation models and the associated notations. In particular, we describe parameters of the state process model and how they link birth and adult recruitments and age- and sex-specific survival probabilities and adult sex ratio with covariates in Sections 4.1 to 4.2. Accurate estimation of birth and adult recruitments and age- and sex-specific survival probabilities and sex ratio is therefore a crucial step in developing the state-space model. As a result, the model explicitly allows for the dependence of birth and adult recruitments and age- and sex-specific survival probabilities and sex ratio on food availability and quality, density-dependent intraspecific competition for food and large carnivore predation. Influences of these factors are indexed by past rainfall, minimum and maximum temperatures and their interactions, prior total population size and environmental seasonality.

The relatively large number of parameters considerably complicates their estimation using classical techniques. We overcome this difficulty using a flexible Bayesian state-space model and present forms of the prior and full conditional distributions in Sections 4.4 and 5 and in Web Appendix G.

3.1 The age and sex structured state-space model–process model

To construct the age- and sex-structured state-space model we first introduce notations for the different topi age and sex classes at time t of the observation process as follows. We assume throughout that all births or recruitments occur at the end of each month. $new(t)$ = observed number of newborns, $q(t)$ = observed number of quarter-sized animals, $h(t)$ = observed number of half-yearlings, $f(t)$ = observed number of adult females, $m(t)$ = observed number of adult males. The state process involves the same age and sex classes. The true but unknown numbers of animals in each age and sex class are denoted by $New(t)$ = actual number of newborns, $Q(t)$ = actual number of quarters, $H(t)$ = actual number of half-yearlings, $F(t)$ = actual number of adult females, $AM(t)$ = actual number of adult males.

3.2 Assigning topi to actual ages in months

Since the exact age of topi is hard to determine through visual field observation, animals were only assigned to age and sex classes. However, the probability of survival likely varies with age and other temporally varying covariates, such as rainfall. For example, a newborn topi must survive the first month of its life to join the quarter-size class. Likewise, a quarter-size topi must survive through 5 consecutive months before graduating to the half-yearling class. So, we assign topi in the quarter and half-yearling age classes to actual ages in months as follows. $Q(t, k)$ = Number of individuals in the quarter-size class with actual ages lying between $k - 1$ and k ($k - 1$ included but k excluded), $k = 2, \dots, 6$ months; $H(t, k)$ = Number of individuals in the half-yearling class with actual ages lying between $k - 1$ and k ($k - 1$ included but k excluded), $k = 7, \dots, 19$ months. Note that $Q(t) = \sum_{k=1}^6 Q(t, k)$ and $H(t) = \sum_{k=1}^{19} H(t, k)$.

For adult females, tracking the reproductive cycle is essential for understanding population dynamics. Young topi start reproducing at about 19 months of age. The topi reproductive cycle spans 11 months, including 8 months for gestation and 3 months for lactation. We assume that a female cannot conceive during this 11-month period. If pregnancy is prematurely terminated, however, then a fresh conception may occur within the 11-month period. But we do not have data to estimate the probability that a pregnant female topi fails to carry pregnancy to term and so do not consider it in the model. We track the pregnancy status of adult females in each of the the 11 months spanned by the reproductive cycle as

follows: $AF(t, \ell)$ = Number of adult females at time t , that gave birth exactly ℓ months ago, $\ell = 1, \dots, 11$; $AF(t, 12)$ = Number of adult females at time t , that gave birth at least 12 months ago.

The adult males $AM(t)$ are not split into subgroups. Male and female half-yearlings at time $t - 1$, denoted by $H(t - 1, 19)$, that join the adult class at time t , are denoted by $NAM(t)$ and $NAF(t)$, respectively. We denote by $R_c(t)$ the probability that an individual graduating from the half-yearling class to the adult class is a female at time t (henceforward referred to as sex ratio). $NAF(t)$ is therefore the number of new adult female recruits that can conceive at time t and give birth 8 months later. So, we add the new adult female recruits to $AF(t, 3)$, the number of adult females that gave birth exactly three months ago, and track future changes in the resulting total number. Note that $F(t) = \sum_{\ell=1}^{12} AF(t, \ell)$. From the preceding definitions, it follows that a total of only $AF(t, 11) + AF(t, 12)$ females can conceive at time t . All these processes are illustrated diagrammatically in Figure 1.

3.3 Stochastic topi population dynamics

The stochastic topi population dynamics model for time $t = 2, \dots, T$ can then be cast as in Table 1. As defined before, $AF(t, 1)$ is the number of females that gave birth exactly one month ago. We assume that the number of females that gave birth at time $t - 1$ is the same as the number of newborns recorded at time $t - 1$. This is a slight underestimate because of unobservable calf mortalities. The population dynamics of adult females is thus modelled as given in Table 1.

3.4 Initialising population size for topi age and sex classes

The time $t = 0$ for our data corresponds to June 1989, one month before the start of the ground sample surveys. To model population size at time $t = 1$, we need to know the initial population size at time $t = 0$. We denote the initial population distribution by New_0 = Number of newborns at time $t = 0$; $Q_0(k)$ = Number of quarters of age k at time $t = 0$, $1 \leq k \leq 6$; $H_0(k)$ = Number of half-yearlings of age k at time $t = 0$, $1 \leq k \leq 19$; $AF_0(k)$ = Number of adult females that gave birth k months before time $t = 0$; AM_0 = Number of adult males at time $t = 0$.

The initial states for the different age and sex classes at time $t = 0$ (namely, $AF_0(k)$, $1 \leq k \leq 12$; AM_0 , etc.) are assumed to follow normal distributions with means determined by the estimated population age and sex structure at the initial

time $t = 0$ and variances assumed to be all equal to 20,000. The distributions of the rest of the initial states are given in Table 1.

We used the aerial and ground survey data to estimate the unknown age and sex structure of the initial population. First, we selected the ground sample counts for the month of June. We calculated the proportion of animals in all the different age and sex classes in each of the 15 years spanning 1989 to 2003 and averaged the proportion for each age and sex class across all the 15 years. We used this average to represent the population proportion for each age and sex class at time $t = 0$ for the month of June. To derive the initial population size estimate for each age and sex class, we multiplied the total population size estimated from the aerial survey data at time $t = 0$ (June 1989) with the average proportion for each age and sex class for June. We use these initial population size estimates for each age and sex class as the means of the normal distributions for the corresponding initial states, New_0 , AM_0 , etc.

3.5 Integrating aerial survey data with demographic ground count data

We integrate the total population size estimates for the entire Masai Mara Ecosystem derived from the aerial surveys with the monthly demographic vehicle ground counts for the Masai Mara Reserve. This enables us to predict the total monthly population size estimates for the entire Masai Mara Ecosystem and for each of its four constituent zones. Let $B_t = New(t) + Q(t) + H(t) + F(t) + M(t)$ be the total topi population size for the Mara Reserve and T_t be the total topi population for all the four zones that collectively constitute the Mara Ecosystem. We further assume that $T_t = K_t B_t$, where K_t is the proportion $\frac{T_t}{B_t}$ at time t . We integrate T_t with the model for ground counts as follows.

$$\begin{aligned}\lambda_t^T &\sim \text{Gamma}\left(\frac{(K_t B_t)^2}{\sigma_T^2}, \frac{K_t B_t}{\sigma_T}\right) \\ T_t &\sim \text{Poisson}(\lambda_t^T)\end{aligned}\tag{1}$$

3.6 Observation process model

The hidden states $(New(t), Q(t), H(t), F(t), M(t))$ are linked to the observed counts $(new(t), q(t), h(t), f(t), m(t))$ assuming Poisson distributions as described in Table 1. We assume that $new(t)$ has expected value $New(t)$. But

some newborn topi are almost certainly missed during the ground surveys because topi hide their young for some time soon after birth, large carnivores kill some newborns whereas others may simply be missed due to visibility bias. To account for potential underestimation, we multiplied $new(t)$ with a correction factor of 1.7, based on experimentation, before determining birth rates in Section 4.2. More generally, however, sightability bias in $new(t)$ can be modeled by allowing $new(t)$ to follow a Poisson distribution with parameter $\frac{\lambda_1(t)}{h(t)}$, where $h(t)$ is a proportionality factor.

4 Predicting expected number of animals in each age and sex class using simultaneous linear equations

We used an interdependent system of linear regression equations (Theil, 1971) to estimate the expected total number of animals in each age and sex class present in the ground sample in each month for use in determining initial population size estimates. The current month endogenous variables appear as regressors in equations for other age or sex classes in the system of simultaneous equations. The model accounts for potential correlation of errors for the set of related regression equations to improve the efficiency of parameter estimates. The modelling framework uses estimation procedures that produce consistent and asymptotically efficient estimates for the system of linear regression equations. We imposed linear restrictions on some of the parameter estimates.

4.1 Notations for predictors of birth recruitment and survival rates

Denoting time by t and the 174 months covered by the vehicle ground counts by $t = 1, \dots, 174$, we introduce a set of notations for the covariates used to model topi birth and adult recruitments, age-specific survival rates and adult sex ratio. The notations and their descriptions are summarized in Table 2.

4.2 Determining the birth recruitment, sex ratio and age-specific survival functions

The method used to determine the functional forms of the relationships between the birth and adult recruitments, sex ratio and age-specific survival rates and the various covariates is described in Web Appendix F. The functional forms of the logit regression models relating birth and adult recruitments and age-specific survival rates and adult sex ratio to covariates are given by the equations in Table 3.

4.3 Determining predation risk

The birth and survival rates are adjusted for environmental seasonality and seasonality in predation risk. During the dry season (July-October) migratory herbivores occupy the Mara, generating a superabundance of food for large predators thereby considerably reducing predation risk for resident large herbivores, such as topi. So, we assume, based on parameter tuning, that predation risk for topi during the dry season is 70% of the risk during the wet season when the migrants are absent from the Mara. Also, adult male topi often fight each other and defend mating territories, potentially elevating their susceptibility to predation. Thus, we assume, also based on parameter tuning, that the survival rate for adult males is 99.7% that of adult females.

4.4 Prior distributions

The prior distributions for the regression coefficients $\gamma^S = (\gamma_1^S, \dots, \gamma_9^S)$, $\gamma^R = (\gamma_1^R, \dots, \gamma_9^R)$, $\gamma^Q = (\gamma_1^Q, \dots, \gamma_{14}^Q)$, $\gamma^Y = (\gamma_1^Y, \gamma_2^Y, \gamma_3^Y)$ and $\gamma^A = (\gamma_1^A, \dots, \gamma_9^A)$ of the logit regression models are assumed to be normal with the same means and diagonal covariance matrices with diagonal elements equal to the estimated covariance components for the corresponding regression coefficient estimates for models in Table 3. The empirical choice of the priors ensures good mixing of the MCMC chains.

We assumed a prior on σ^2 in Section 3.5 following a gamma distribution, Gamma(50,000, 0.000001), which has a very large average variance for topi population size of 50,000,000,000. Prior distributions for the initial states (New_0 , $Q_0(k)$, etc.) are specified in Section 3.4. The prior on K_t is taken to be Beta(5402.23, 4182.9). This prior is determined by using the empirical proportions of the total topi population size in each of the four zones constituting the Masai Mara

Ecosystem derived from the aerial survey monitoring data for July 1989 to December 2003. The Dirichlet distribution is fitted to the data on proportions and Maximum Likelihood estimates of its parameters are obtained using the “DirichletReg” package in R. The marginal beta distribution of the Dirichlet distribution is obtained as Beta(5402.23, 4182.9). σ_T is fixed at 1906.42, the average standard deviation of the topi population size estimates for the Mara Ecosystem based on the aerial survey data for July 1989 to December 2003.

5 Full conditional distributions and convergence of MCMC chains

The forms of the full conditional distributions of $New(t)$, $Q(t, k)$, $H(t, k)$, $NAF(t)$, $NAM(t)$ and other parameters are presented in Web Appendix G. The functional forms of the full conditional distributions of γ^R , γ^Q , γ^Y and γ^A (collectively referred to as γ 's) and other parameters are also presented in Web Appendix G.

The functional forms of the full conditional distributions for the γ 's are not conformable to Gibbs sampling. Moreover, the resulting Metropolis-Hastings chain for the γ 's converge quite slowly, making the algorithm highly inefficient. To accelerate the rate of convergence of the chain we implement Transformation Markov Chain Monte Carlo (TMCMC) at the Metropolis-Hastings step. A theoretical discussion of TMCMC can be found in Dutta and Bhattacharya (2014). Details on how TMCMC was specialized for our chain are discussed in Web Appendix H. The MCMC simulations were continued for 1,500,000 iterations after discarding the initial 500,000 iterations. The convergence of the MCMC chains for each parameter was assessed informally using trace plots. All the trace plots show evidence of convergence and are provided in Web Figures 1 and 2.

5.1 Model validation using balanced bootstrap sampling

To establish robustness of the model, we performed a model validation test using balanced bootstrap samples. We first drew 10 different samples from each of the 75 aerial surveys conducted between 1977 and 2018 using balanced bootstrap sampling. The balanced bootstrap selection was performed by using the algorithm of Gleason (1988) in SAS PROC SURVEYSELECT. The balanced bootstrap method was used to select 10 samples from each of the total of 75 aerial surveys with equal probability and with replacement, where each aerial survey

had 232 to 705 sampling units each measuring $5 \text{ km} \times 5 \text{ km}$, $2.5 \text{ km} \times 5 \text{ km}$ or $10 \text{ km} \times 5 \text{ km}$. Because the bootstrap selection is balanced the overall total number of selections is the same for each sampling unit (Davison et al., 1986). We then estimated the total topi population size for each bootstrap sample using Jolly’s Method 2 (Jolly, 1969) for transects of unequal lengths.

5.2 Cross-validation results

Before running the model to produce the parameter estimates and interpreting their significance, we validated the model to establish its suitability for predicting population dynamics. The estimates of population sizes from the bootstrap samples served as the actual population size of a hypothetical topi population. Using these estimates, we generated a set of 10 time series of hypothetical ground survey data each of length 174 months and having the same age and sex classes as the actual ground sample count data (further details in Web Appendix I). We call these hypothetical ground data sets generated data and the corresponding population size estimates bootstrap population estimates. We then fit our model separately to each of the generated data and obtained estimates of total population size and the corresponding 95% credible limits of the estimates from the state process model in Section 3.1. We call these estimates generated estimates. Next, we compare the bootstrap population estimates with the generated estimates by observing whether the bootstrap estimates lie within the 95% credible limits of the generated estimates for each of the 10 bootstrap population time series. However, running the model separately for each time series is computationally very expensive. To reduce the computing time we used the idea behind the Importance Resampling MCMC (IRMCMC) proposed by Bhattacharya and Haslett (2007). Though developed for inverse problems, this method can be generalised to tackle the current problem. The precise details of this generalization are discussed in Web Appendix I.1. We ran our model using IRMCMC for each of the generated data sets (10 time series) and calculated the percentage coverage of the bootstrap populations at each of the 174 time points. The coverages for the 10 time series of bootstrap samples vary from 85% to 97%. The bespoke R code written in R software version 4.1.1, used to implement the population dynamics model is provided in Web Appendices P and Q, whereas the SAS codes used to fit the simultaneous linear equations and relate birth recruitment and survival rates and adult sex ratio to the covariates are provided in Web Appendix R.

6 Results

6.1 Topi population trajectory by age and sex class

The model captures the essential and well-known features of the Mara topi population dynamics. First, it accurately captures the declining population trajectory of all the age and sex classes; adult female, adult male, half-yearling, quarter-size and newborn topi in the Mara between 1989 and 2003 (Figures 2 and 3). Second, it accurately tracks inter-annual variation in the reproductive seasonality, phenology, synchrony and prolificacy of topi births and juvenile recruitment (Figure 2; Sinclair et al., 2000; Ogutu et al., 2010, 2011). Figures 2 and 3 show the observed and predicted population sizes for each age and sex class for each of the 174 observation points (July 1989–December 2003) and the associated 95% credible limits averaged across the 1,500,000 MCMC simulation replications. The 95% credible intervals for the predicted values are not too wide indicating convergence of the MCMC chains. The birth recruitment rates (Figures 2 and Web Figure 5a) show strong seasonality consistent with the pronounced reproductive seasonality characteristic of the Mara-Serengeti topi. Further, the prolificacy of topi births is strongly time-varying, reflecting the controlling influence of the seasonally and inter-annually varying rainfall (Ogutu et al., 2014, 2015). The pronounced seasonality in prolificacy of births and birth recruitment also carry over to the trajectories of the quarter and half-yearling size classes (Figures 2b–c) but not to the adult age class (Figures 3a–b). The persistent declines in the trajectories of topi birth recruitment, quarter and half-yearling classes, adult males and females and the overall topi population size are consistent with the overall topi population decline in the Mara Ecosystem from 1977 to 2018 (Figure 3c; Ogutu et al., 2016; Veldhuis et al., 2019). Finally, there is evident seasonality in the overall topi population trajectory generated by the strong seasonality of births and juvenile recruitment in the ecosystem (Figure 3c).

6.2 Adult female recruitment and females available to conceive

Adult female recruitment is strongly seasonal, consistent with the seasonality in births and juvenile recruitment. The expected number of new adult females recruited into the population per month peaked in 1989–1990 but was noticeably lower in the other years (Web Figure 3a). Moreover, the number of adult females that gave birth exactly 8 months ago (Web Figure 3b) and the number of adult fe-

males that were available to conceive (Web Figure 3c) decreased persistently and markedly. The latter reduced from a maximum of nearly 4,000 in 1989 to around 2,000 animals by 2003 (Web Figure 3c). Thus, the decline in newborns was associated with a persistent decline in the number of adult females. Notably also, the severe 1993 drought resulted in evidently fewer adult females (in 1994) that gave birth in 1993 (Web Figure 3b) or that were available to conceive in 1994–1995 (Web Figure 3c).

6.3 Temporal variation in age structure and adult sex ratio

The expected population proportions of newborns, quarter-size and half-yearlings all tended to increase as the topi population decreased but the proportion of the adult population segment remained rather constant over time apart from sustained seasonal oscillations from 1989 to 2003 (Web Figures 4a–d).

6.4 Factors influencing birth recruitment and survival rates and adult sex ratio

The posterior means, standard deviations and 95% credible intervals for parameters of the models relating birth and adult recruitments, survival rates and adult sex ratio to various covariates are summarized in Web Tables 4–8. Similarly, posterior densities for a sample of the parameters are displayed in Web Figures 7–10. There was evident seasonality in birth recruitment and survival of quarter-size, half-yearling and adult topi (Web Figures 5a–d). Birth recruitment was negatively density-dependent for the declining topi population and was also influenced by prior rainfall and average temperatures (Web Table 4). Besides seasonality, quarter-size survival was influenced only by prior rainfall (Web Table 5). Half-yearling survival fluctuated seasonally and was apparently influenced only by past rainfall (Web Table 6). Lastly, adult survival was negatively density-dependent and also varied with past rainfall amounts (Web Table 7). Adult sex ratio varied seasonally and with rainfall, minimum and maximum temperatures but was apparently not density-dependent (Web Table 8).

6.5 Birth recruitment rates, survival rates and sex ratio

The estimated birth recruitment, survival rates and sex ratios are consistent with expectation and are displayed in Web Figures 5–6. Topi birth recruitment was

strongly seasonal, unusually low during the 1993-1994 drought and the highest during 1994-1995 with good rainfall (Web Figure 5a). The survival rates for quarter size (Web Figure 5b), half-yearling (Web Figure 5c) and adult (Web Figure 5d) topi age classes showed strong and sustained seasonality. Adult survival was the lowest during 1999–2001, coincident with the extreme 1999–2000 drought (Web Figure 5d). The proportion of adult females increased from a monthly maximum of 59% to 64% whereas the proportion of adult males decreased correspondingly from a peak of about 41% to 35% between 1989 and 2003 (Web Figures 6a–b).

6.6 Comparing predicted topi population size with aerial survey data

Fourteen of the 75 DRSRS aerial surveys for the Masai Mara Ecosystem for 1977–2018 (Section 2.2) fell within the period spanned by the ground survey data (July 1989–December 2003). The total population size estimates from these 14 aerial surveys were in reasonable agreement with the total topi population size predicted by the Bayesian state-space model. Notably, the estimated total topi population size was within the 95% confidence limits of most of the total population size estimates derived from the 14 DRSRS aerial surveys (Figure 3). Moreover, trends in the estimated topi population size for each of the four zones constituting the Mara ecosystem (Web Figures 11a–d) are also in good agreement with the corresponding aerial total population size estimates and show that topi numbers worryingly declined persistently throughout the Mara Ecosystem regardless of the degree of protection – highest in the Mara Reserve, intermediate in the conservancies and lowest in the unprotected agro-pastoral lands of Siana and the Loita Plains. However, topi were substantially more abundant in the protected reserve and semi-protected conservancies than in the unprotected agro-pastoral lands.

7 Discussion

We develop a flexible and general, integrated state-space model in a Bayesian framework for estimating large herbivore population demographic parameters, dynamics and the associated uncertainties. The model is illustrated using the Mara-Serengeti topi population inhabiting the World-famous Greater Mara-Serengeti Ecosystem of Kenya and Tanzania in East Africa. The state-space model allows estimation of both process and observation error variances (De Valpine and Hastings, 2002; Buckland et al., 2004). The model incorporates age and sex structure and

key life-history characteristics (e.g., gestation length, lactation period, pregnancy status, females available to conceive, one young per birth event) and life-history strategies (e.g. feeding style, grazer for topi, and foraging style, resident for topi) essential to understanding large herbivore population dynamics and efficiently integrates ground demographic survey with aerial survey data. We relate birth and adult recruitments and age-class specific survival rates and adult sex ratio to various covariates, such as prior population density, predation risk, past rainfall and temperature, environmental seasonality and their interactions. To estimate model parameters, we used the MCMC method in a Bayesian framework because of its flexibility (Brooks et al., 2004; Hoyle and Maunder, 2004; Schaub et al., 2007; Finke et al., 2019). The convergence of the MCMC chains of the parameters is accelerated using the Transformation MCMC (TMCMC) technique (Dutta and Bhattacharya, 2014) and the idea behind IRMCMC (Bhattacharya and Haslett, 2007) to reduce the computational time for model validation.

The predicted population trajectories show persistent and marked declines in the Mara topi population from 1989 to 2003 in accord with the trends derived from aerial surveys for 1977–2018 (Ogutu et al., 2016; Veldhuis et al., 2019). Importantly, whereas birth and adult recruitments fluctuated around a stable average, the survival rates for quarter size, half-yearling size and adults decreased gradually and contemporaneously with the overall topi population decline. The disturbing and sustained decline in numbers of topi and other species in the Mara and across Kenya (Ogutu et al., 2016) and continental Africa (Craigie et al., 2010) increases the urgency for establishing their leading causes and developing effective population conservation and recovery strategies.

The modelling framework can be extended to (i) identify the most influential processes driving population declines and assess their relative importance, (ii) test interesting ecological hypotheses, (iii) enable rigorous forward-projection of large herbivore population dynamics allowing for both parameter and future demographic uncertainty (Hoyle and Maunder, 2004). Further extension can also (iv) enable assessment of likely future populating trajectories under various scenarios of climate change, land use change, socio-economic development, human population growth, livestock population density, conservation and management interventions, such as formation of new wildlife conservancies (Rhodes et al., 2011; Maunder et al., 2015; Mosnier et al., 2015). Moreover, the monthly time step allows the model outputs to be used to study potential shifts in reproductive seasonality, phenology, synchrony and prolificacy of births, juvenile recruitment and adult sex ratio (Ogutu et al., 2010; 2011, 2014, 2015) in response to future changes in climate and other factors. It would also be interesting and useful to

adapt the model for other species, with contrasting life-history traits and strategies as well as trophic relations, such as hartebeest (*Alcelaphus buselaphus cokeii*), impala (*Aepyceros melampus*), waterbuck (*Kobus ellipsyrimnus*), zebra, warthog (*Phorcocoerus africana*) and giraffe (*Giraffa camelopardalis*).

The model can also be extended to include several additional features. First, females that are reproducing for the first time can be allowed to have a lower pregnancy rate (86%) than older (100%) females (Duncan, 1975). Second, females that lose their calves soon after birth can be moved to the group of females available to conceive. Third, the survival rate of calves aged 0 to 1 month can be explicitly incorporated in the model, especially if empirical estimates of such rates can be obtained. Fourth, the dependence of birth recruitment and age-specific survival rates and sex ratio on covariates may alternatively be made time-varying to potentially better account for temporal variation in the influence of the covariates. Fifth, the model can be made spatially explicit to allow for spatial variation in the type and intensity of factors influencing survival and recruitment rates and sex ratio. Sixth, sightability bias in newborns, $new(t)$, can be modeled explicitly by specifying $new(t)$ to follow a Poisson distribution with parameter $\lambda_1(t)/h(t)$, where the proportionality constant $h(t)$ is sampled from a suitable probability distribution. Seventh, birth recruitment and survival rates and sex ratio can be related to additional covariates, particularly anthropogenic covariates, such as human population density, livestock population density, settlement density and progressive habitat loss. Lastly, birth recruitment, survival rates and sex ratio can all be related to one set of covariates collected at the monthly time scale using the ground demographic data whereas the inter-annual variation in the overall population growth rate can be related to the other set of covariates collected at the annual time scale using the aerial survey data.

Acknowledgements

The ground surveys were funded by the World Wide Fund for Nature–East Africa Program (WWF–EARPO) and Friends of Conservation (FOC) and the aerial surveys by the Kenya Government through the DRSRS. This project has received funding from the European Union’s Horizon 2020 research and innovation programme under Grant Agreement No. 641918. JOO was additionally supported by a grant from the German Research Foundation (DFG; Grant # 257734638). Further information on acknowledgment (data generation and provision, permissions, additional financial and logistical support, etc) is provided in Web Appendix O.

References

- Besbeas, P., Freeman, S. N., and Morgan, B. J. (2005). The potential of integrated population modelling. *Australian and New Zealand Journal of Statistics* **47**, 35–48.
- Bhattacharya, S. and Haslett, H. (2007). Importance re-sampling MCMC for cross-validation in inverse problems. *Bayesian Analysis* **2**, 385–408.
- Boutton, T. W., Tieszen, L. L., and Imbamba, S. K. (1988a). Biomass dynamics of grassland vegetation in Kenya. *African Journal of Ecology* **26**, 89–101.
- Boutton, T. W., Tieszen, L. L., and Imbamba, S. K. (1988b). Seasonal changes in the nutrient content of East African grassland vegetation. *African Journal of Ecology* **26**, 103–115.
- Brooks, S. P., King, R., and Morgan, B. J. T. (2004). A Bayesian approach to combining animal abundance and demographic data. *Animal Biodiversity and Conservation* **27**, 515–529.
- Buckland, S. T., Newman, K. B., Fernández, C., Thomas, L., and Harwood, J. (2007). Embedding population dynamics models in inference. *Statistical Science* **22**, 44–58.
- Buckland, S. T., Newman, K. B., Thomas, L., and Koesters, N. B. (2004). State-space models for the dynamics of wild animal populations. *Ecological Modelling* **171**, 157–175.
- Ceballos, G., Ehrlich, P. R., and Dirzo, R. (2017). Biological annihilation via the ongoing sixth mass extinction signaled by vertebrate population losses and declines. *Proceedings of National Academy of Sciences* **114**, E6089–E6096.
- Chase, M. J., Schlossberg, S., Griffin, C. R., Bouché, P. J. C., Djene, S. W., Elkan, P. W., Ferreira, S., Grossman, F., Kohi, E. M., Landen, K., Omondi, P., Peltier, A., Selier, S. A. J., and Sutcliffe, R. (2016). Continent-wide survey reveals massive decline in African savannah elephants. *PeerJ* **4**, e2354.
- Craigie, I. D., Baillie, E. M., Balmford, A., Carbone, C., Collen, B., Green, R. E., and Hutton, J. M. (2010). Large mammal population declines in Africa’s protected areas. *Biological Conservation* **143**, 2221–2228.

- Davison, A. C., Hinkley, D. V., and Schechtman, E. (1986). Algorithms for balanced bootstrap simulations. *Biometrika* **73**, 555–566.
- De Valpine, P. and Hastings, A. (2002). Fitting population models incorporating process noise and observation error. *Ecological Monographs* **72**, 57–76.
- Deshmukh, I. K. (1984). A common relationship between precipitation and grassland peak biomass for East and Southern Africa. *African Journal of Ecology* **22**, 181–186.
- Duncan, P. (1975). *Topi and their Food Supply*. PhD dissertation, University of Nairobi, Kenya.
- Dutta, S. and Bhattacharya, S. (2014). Markov Chain Monte Carlo based on deterministic transformations. *Statistical Methodology* **16**, 100–116.
- Estes, R. D. (1991). *The Behavior Guide to African Mammals: Including Hoofed Mammals, Carnivores, Primates*. University of California Press.
- Finke, A., King, R., Beskos, A., and Dellaportas, P. (2019). Efficient sequential monte carlo algorithms for integrated population models. *Journal of Agricultural, Biological and Environmental Statistics* **24**, 204–224.
- Funk, C., Peterson, P., Landsfeld, M., Pedreros, D., Vermin, J., Shukla, S., Husak, G., Rowland, J., Harrison, L., Hoell, A., and Michaelsen, J. (2015). The climate hazards infrared precipitation with stations—a new environmental record for monitoring extremes. *Scientific Data* **2**, doi:10.1038/sdata.2015.66.
- Gleason, J. R. (1988). Algorithms for balanced bootstrap simulations. *American Statistician* **42**, 263–266.
- Hoyle, S. D. and Maunder, M. N. (2004). A Bayesian integrated population dynamics model to analyze data for protected species. *Animal Biodiversity and Conservation* **27**, 247–266.
- Jolly, G. M. (1969). Sampling methods for aerial censuses of wildlife populations. *East African Agricultural and Forestry Journal* **34**, 46–49.
- Maunder, M. N., Deriso, R. B., and Hanson, C. H. (2015). Use of state-space population dynamics models in hypothesis testing: advantages over simple log-linear regressions for modeling survival, illustrated with application to longfin smelt (*spirinchus thaleichthys*). *Fisheries Research* **164**, 102–111.

- McCallum, M. L. (2015). Vertebrate biodiversity losses point to a sixth mass extinction. *Biodiversity and Conservation* **24**, 2497–2519.
- Mosnier, A., Doniol-Valcroze, T., Gosselin, J. F., Lesage, V., Measures, L. N., and Hammill, M. O. (2015). Insights into processes of population decline using an integrated population model: The case of the St. Lawrence estuary beluga (*delphinapterus leucas*). *Ecological Modelling* **314**, 15–31.
- Mukhopadhyay, S., Ogutu, J. O., Bartzke, G. S., Dublin, H. T., and Piepho, H. P. (2019). Modelling spatio-temporal variation in sparse rainfall data using a hierarchical Bayesian regression model. *Journal of Agricultural, Biological and Environmental Statistics* **24**, 369–393.
- Newman, K. B., Buckland, S. T., Morgan, B. J., King, R., Borchers, D. L., Cole, D. J., Besbeas, P., Gimenez, O., and Thomas, L. (2014). *Modelling Population Dynamics*. Springer, New York.
- Newman, K. B., Buckland, T. B., Lindley, S. T., Thomas, L., and Fernández, C. F. (2006). Hidden process models for animal population dynamics. *Ecological Applications* **16**, 74–86.
- Newman, K. B., Fernández, C., Thomas, L., and Buckland, S. T. (2009). Monte Carlo inference for state-space models of wild animal populations. *Biometrics* **65**, 572–583.
- Ogutu, J. O., Piepho, H. P., and Dublin, H. T. (2014). Responses of phenology, synchrony and fecundity of breeding by African ungulates to interannual variation in rainfall. *Wildlife Research* **40**, 698–717.
- Ogutu, J. O., Piepho, H. P., and Dublin, H. T. (2015). Reproductive seasonality in African ungulates in relation to rainfall. *Wildlife Research* **41**, 323–342.
- Ogutu, J. O., Piepho, H. P., Dublin, H. T., Bhola, N., and Reid, R. S. (2008). El Niño Southern Oscillation (ENSO), rainfall, temperature and Normalized Difference Vegetation Index (NDVI) fluctuations in the Mara–Serengeti Ecosystem. *African Journal of Ecology* **46**, 132–143.
- Ogutu, J. O., Piepho, H. P., Dublin, H. T., Bhola, N., and Reid, R. S. (2010). Rainfall extremes explain interannual shifts in timing and synchrony of calving in topi and warthog. *Population Ecology* **52**, 89–102.

- Ogutu, J. O., Piepho, H. P., Dublin, H. T., Bhola, N., and Reid, R. S. (2011). Dynamics of births and juvenile recruitment in Mara-Serengeti ungulates in relation to climatic and land use changes. *Population Ecology* **53**, 195–213.
- Ogutu, J. O., Piepho, H. P., Said, M. Y., Ojwang, G. O., Njino, L. W., Kifugo, S. C., and Wargute, P. W. (2016). Extreme wildlife declines and concurrent increase in livestock numbers in Kenya: What are the causes? *PLoS ONE* **11**, e0163249.
- Rhodes, J. R., Ng, C. F., de Villiers, D., Preece, H. J., McAlpine, C. A., and Possingham, H. P. (2011). Using integrated population modelling to quantify the implications of multiple threatening processes for a rapidly declining population. *Biological Conservation* **144**, 1081–1088.
- Schaub, M., Gimenez, O., Sierro, A., and Arlettaz, R. (2007). Use of integrated modeling to enhance estimates of population dynamics obtained from limited data. *Conservation Biology* **21**, 945–955.
- Sinclair, A. R. E., Mduma, S. A., and Arcese, P. (2000). What determines phenology and synchrony of ungulate breeding in Serengeti? *Ecology* **81**, 2100–2111.
- Skinner, J. D. and Chimimba, C. T. (2005). *The Mammals of the Southern African Subregion*. Cambridge University Press, Cambridge.
- Stelfox, J. G., Peden, D. G., Epp, H., Hudson, R. J., Mbugua, S. W., Agatsiva, J. L., and Amuyunzu, C. L. (1986). Herbivore dynamics in southern Narok, Kenya. *The Journal of Wildlife Management* **50**, 339–347.
- Theil, H. (1971). *Principles of Econometrics*. John Wiley and Sons, New York.
- Thomas, L., Buckland, S. T., Newman, K. B., and Harwood, J. (2005). A unified framework for modelling wildlife population dynamics. *Australian and New Zealand Journal of Statistics* **47**, 19–34.
- Trenkel, V. M., Elston, D. A., and Buckland, S. T. (2000). Fitting population dynamics models to count and cull data using sequential importance sampling. *Journal of the American Statistical Association* **95**, 363–374.
- Veldhuis, M. P., Ritchie, M. E., Ogutu, J. O., Morrison, T. A., Beale, C. M., Estes, A. B., and Wargute, P. W. (2019). Cross-boundary human impacts compromise the Serengeti-Mara Ecosystem. *Science* **363**, 1424–1428.

- Zhao, Q., Arnold, T. W., Devries, J. H., Howerter, D. W., Clark, R. G., and Weegman, M. D. (2019a). Land-use change increases climatic vulnerability of migratory birds: Insights from integrated population modelling. *Journal of Animal Ecology* **88**, 1625–1637.
- Zhao, Q., Boomer, G. S., and Royle, J. A. (2019b). Integrated modeling predicts shifts in waterbird population dynamics under climate change. *Econography* **42**, 1470–1481.

Supporting Information

Web Appendices, Tables, and Figures referenced in Sections 2–6 are provided in the files Web Appendices A-O.pdf. The R and SAS codes for the method and the simulation are provided in Web Appendix Q.R, Web Appendix Q.P and Web Appendix R.sas. The ground survey dataset is available in TopiData.csv whereas the aerial survey dataset is provided in AerialData.csv.

Table 1: State-space and observation process model formulations. All the notations are explained in Sections 3.1, 3.2, 3.3, 3.6 and 3.4 in the text.

Model	Distributions
<p>State process for newborns, quarter size, half-yearlings, adult females and adult males for time $t = 2, \dots, T$</p>	$New(t) \sim Binomial(AF(t, 11) + AF(t, 12), R_r(t))$ $Q(t, 1) \sim Binomial(New(t-1), s_q(t))$ $Q(t, k) \sim Binomial(Q(t-1, k-1), s_q(t)), k = 3, \dots, 6$ $H(t, 1) \sim Binomial(Q(t-1, 6), s_h(t))$ $H(t, k) \sim Binomial(H(t-1, k-1), s_h(t)), k = 7, \dots, 19$ $(NAF(t), NAM(t)) \sim Multinomial(H(t-1, 19), R_c(t) \times s_a(t), (1 - R_c(t)) \times s_a(t))$ $AM(t) \sim Binomial(AM(t-1) + NAM(t-1), s_a(t))$
<p>State process for breeding adult females for time $t = 2, \dots, T$</p>	$AF(t, 1) \sim Binomial(New(t-1), s_a(t))$ $AF(t, k) \sim Binomial(AF(t-1, k-1), s_a(t)), k = 2, 3$ $AF(t, 4) \sim Binomial(AF(t-1, 3) + NAF(t-1), s_a(t))$ $AF(t, k) \sim Binomial(AF(t-1, k-1), s_a(t)), k = 5, \dots, 11$ $AF(t, 12) \sim Binomial(AF(t-1, 11) + AF(t-1, 12) - New(t-1), s_a(t))$
<p>Initial state process at time $t = 0$</p>	$New_0 \sim Binomial(AF_0(11) + AF_0(12), R_r(t))$ $Q(1, 1) \sim Binomial(New_0, s_q(1))$ $Q(1, k) \sim Binomial(Q_0(k-1), s_q(1)), k = 3, \dots, 6$ $H(1, 1) \sim Binomial(Q_0(6), s_h(1))$ $H(1, k) \sim Binomial(H_0(k-1), s_h(1)), k = 7, \dots, 19$ $(NAF(1), NAM(1)) \sim Multinomial(H_0(19), R_c(1) \times s_a(t), (1 - R_c(1)) \times s_a(t))$ $AM(1) \sim Binomial(AM_0, s_a(1))$ $New(1) \sim Binomial(AF(1, 11) + AF(1, 12), R_r(t))$ $AF(1, 1) \sim Binomial(New_0, s_a(1))$ $AF(1, k) \sim Binomial(AF_0(k-1), s_a(1)), k = 2, 3, \dots, 11$ $AF(1, 12) \sim Binomial(AF_0(11) + AF_0(12) - New_0, s_a(1))$

Table 2: Notations for the covariates used for building the logit models in Table 3 and their descriptions.

Notation for covariate	Description of notation for covariate
$month(t) =$	Calendar month corresponding to January-December and numbered as 1, 2, ..., 12
$rain(7 - 11, t) =$	Average total monthly rainfall including lags 6 to 10 at time t (i.e., 7 to 11 months before the birth month)
$Npop(t) =$	Total topi population size at lag 7 at time t (i.e., around conception time 8 months ago)
$mintemp(t) =$	Minimum temperature at time t
$maxtemp(t) =$	Maximum temperature at time t
$lagmin(\ell, t) =$	Minimum temperature at lag ℓ at time t , $\ell = 1, 2, \dots, 11$ (i.e., up to 4 months pre-conception)
$lagmax(\ell, t) =$	Maximum temperature at lag ℓ at time t , $\ell = 1, 2, \dots, 11$
$Apop(t) =$	Total population size at lag 1 at time t
$lagrain(\ell, t) =$	Total monthly rainfall at lag ℓ at time t , $\ell = 0, 1, 2, \dots, 11$. Note that $lagrain(0, t)$ stands for total monthly rainfall at time t
$wet1(t) =$	Total wet season rainfall at lag 1 (i.e., in the immediately preceding year) at time t
$earlywet1(t) =$	Total early wet season (November–February) rainfall at lag 1 (i.e., in the immediately preceding year) at time t
$dry1(t) =$	Total dry season rainfall at lag 1 (i.e., in the immediately preceding year) at time t
$mavrain(\ell - p, t) =$	Moving average of rainfall between lags ℓ and p ($\ell < p$) at time t

Table 3: Formulations of the relationships between the logits of recruitment and survival rates and covariates. All the notations are explained in Sections 3.1, 3.2, 3.3, 3.4 and 4.1 and in Table 2 in the text. The covariates are explained in Web Table 3. The models were fitted using the SAS Procedure GLIMMIX (Web Appendix R).

Rates	Equation
Birth recruitment	$\log\left(\frac{R_r(t)}{1-R_r(t)}\right) = \gamma_1^R + \gamma_2^R month(t) + \gamma_3^R month^2(t) + \gamma_4^R month^3(t) + \gamma_5^R rain(7-11, t) + \gamma_6^R rain^2(7-11, t) + \gamma_7^R Npop(t) + \gamma_8^R mintemp(t) + \gamma_9^R maxtemp(t)$
Quarter size survival	$\log\left(\frac{s_q(t)}{1-s_q(t)}\right) = \sum_{k=1}^{12} \gamma_k^Q \delta_k(t) + \gamma_{13}^Q dry1(t) + \gamma_{14}^Q mavrain(3-4, t)$
Half-yearling survival	$\log\left(\frac{s_y(t)}{1-s_y(t)}\right) = \sum_{k=1}^{12} \gamma_k^Y \delta_k(t) + \gamma_{13}^Y earlywet1(t)$
Adult survival	$\log\left(\frac{s_a(t)}{1-s_a(t)}\right) = \sum_{k=1}^2 \gamma_k^A \delta_k(t) + \gamma_3^A Apop(t) + \gamma_4^A lagrain(4, t) + \gamma_5^A lagrain(5, t) + \gamma_6^A lagrain(6, t) + \gamma_7^A lagrain(7, t) + \gamma_8^A wet1(t)$
Adult recruitment	$\log\left(\frac{R_c(t)}{1-R_c(t)}\right) = \sum_{k=1}^2 \gamma_k^S \delta_k(t) + \gamma_3^S wet1(t) + \gamma_4^S dry1(t) + \gamma_5^S lagrain(0, t) + \gamma_6^S rain(7-11, t) + \gamma_7^S mintemp(t) + \gamma_8^S lagmin(2, t) + \gamma_9^S lagmax(1, t)$

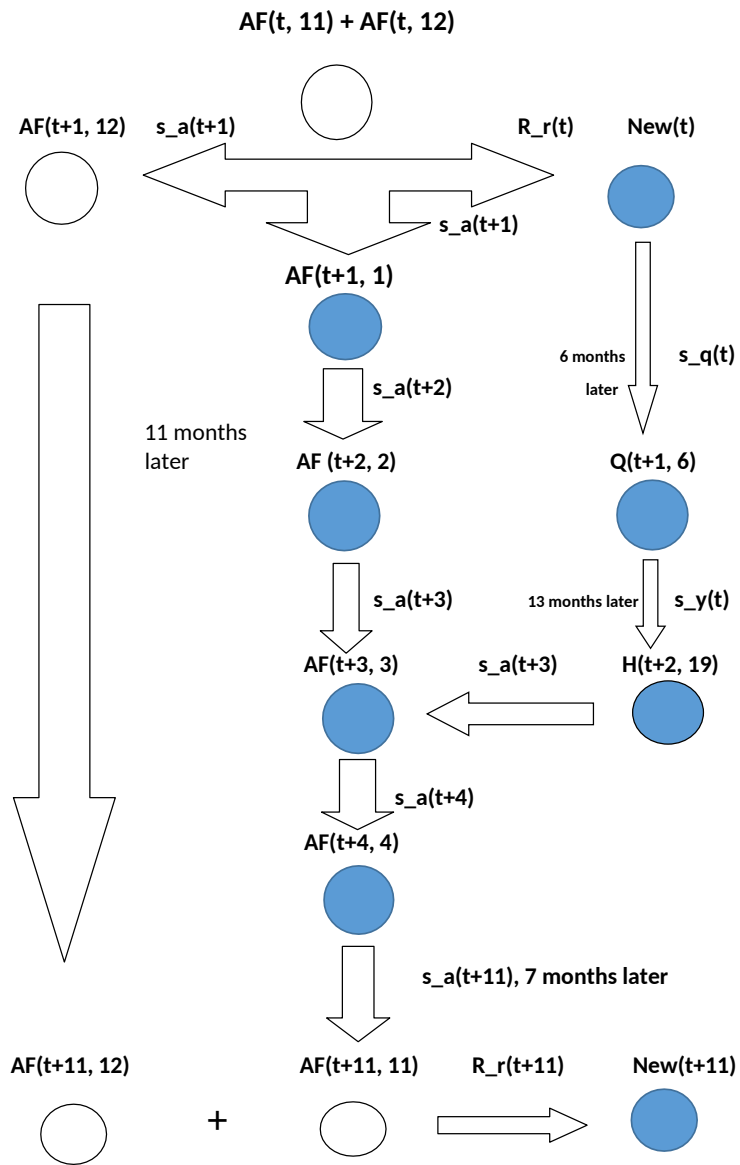


Figure 1: Flow chart showing the reproduction and recruitment processes in topi. The notations are defined in the text.

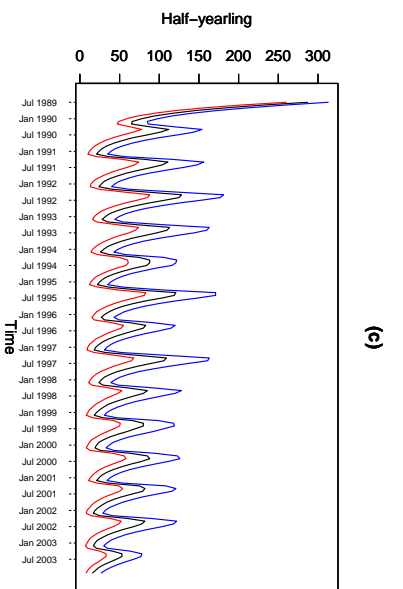
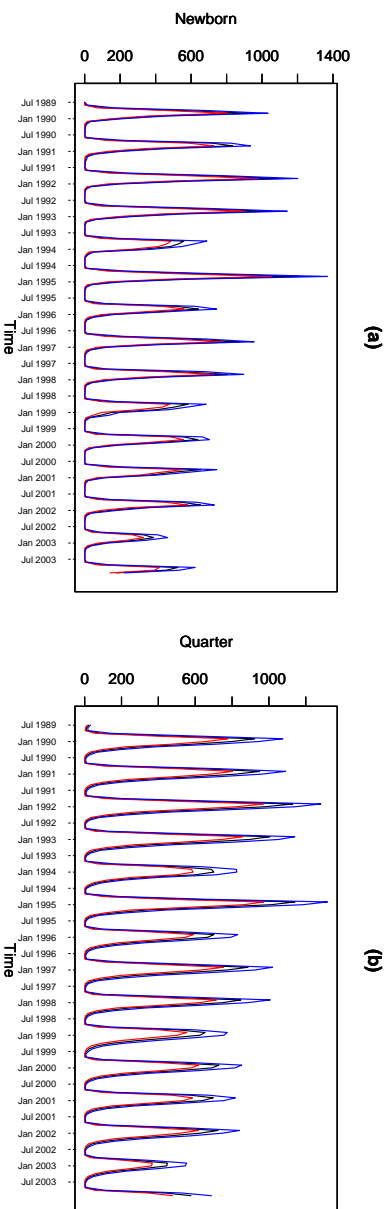


Figure 2: Modelled (black lines) population trajectories and the associated 95% lower (red lines) and upper (blue lines) credible limits for a) newborn, b) quarter and c) half-yearling topi.

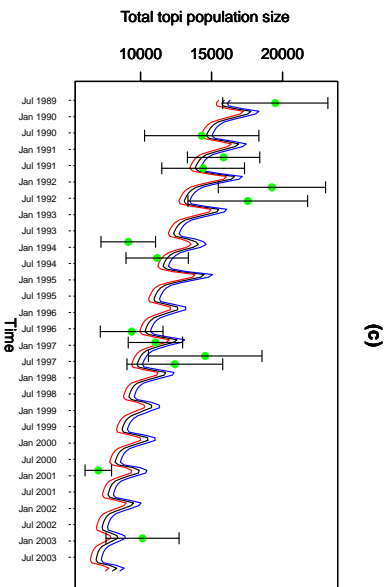
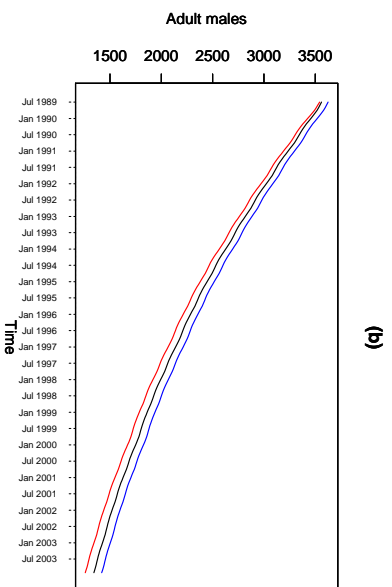
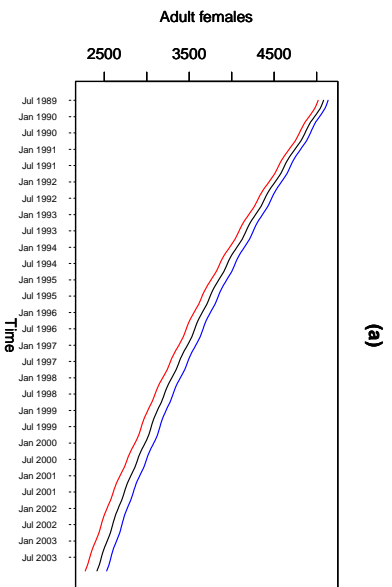


Figure 3: Modeled (black lines) population trajectories and the associated 95% lower (red line) and upper (blue line) credible limits for a) adult female, b) adult male and c) total topi population size overlaid with the population size estimates (green filled circles) and their standard errors (vertical whiskers) based on the DRSRS aerial surveys. The DRSRS population size estimates and their standard errors were multiplied by 1.3 to correct for sightability bias (Stelfox et al., 1986).